Disorder-order transitions in Na_xCoO_2 ($x \sim 0.58$)

Dai Igarashi,* Yuzuru Miyazaki, and Tsuyoshi Kajitani
Department of Applied Physics, Graduate School of Engineering, Tohoku University, 6-6-05 Aramaki Aoba, Aoba-ku, Sendai 980-8579, Japan

Kunio Yubuta
Advanced Research Center of Metallic Glasses, Institute for Materials Research, Tohoku University, 2-1-1 Katahira, Aoba-ku, Sendai 980-8577, Japan

(Received 21 August 2008; published 26 November 2008)

First-order structural transitions have been discovered for a γ-Na_xCoO_2 ($x \sim 0.58$) sample at $T_1 = 235$ K and $T_2 = 288$ K. Based on the combined results of electron and neutron-diffraction experiments, the compound has been revealed to exhibit a $\sqrt{7}a_0 \times \sqrt{7}a_0$-type ($a_0$ represents the a-axis length of the hexagonal basic structure) ordered superstructure with the space group of $P6_3/m$, being isostructural with $K_4Co_7O_{14}$, due to the ordering of Na atoms in this temperature range. The Na ordering triggers a cooperative shift of Co-atom trimers parallel to the c axis, leading to an undulated arrangement of the CoO_2 conduction paths. Anomalous change in the magnetic susceptibility, electrical resistivity, and lattice parameters at T_1 and T_2 can be explained by the slight distortion of the CoO_2 layer. Above T_2, in contrast, the compound turns out to possess the γ-Na_xCoO_2-type structure, in which the Na1 and Na2 atoms are randomly distributed.

DOI: 10.1103/PhysRevB.78.184112 PACS number(s): 64.60.Cn, 61.05.J−, 61.05.fm, 75.30.Kz

I. INTRODUCTION

The layered cobalt oxides γ-Na_xCoO_2 have attracted considerable interest in the last decade due to the successive discovery of the superb thermoelectric properties of an $x \sim 0.70$ sample[1] and the superconductivity of a hydrated $x \sim 0.30$ sample.[2] After these discoveries, Foo *et al.*[3] carefully measured the transport properties of γ-Na_xCoO_2 samples and established an electronic phase diagram. In this system, the valence state of Co ions, being altered with the Na composition x, plays key roles in its structural and physical properties.

Na atoms in the γ-Na_xCoO_2 system occupy two inequivalent sites, namely, Na1 at $2b\,(0,0,1/4)$ and Na2 at $6h\,(x,2x,1/4)$ in a hexagonal unit cell with $P6_3/mmc$ space group and $a_0 \sim 2.82$ Å and $c_0 \sim 10.9$ Å.[4] The Na atoms were considered to be randomly distributed at both sites in almost all compositions. However, at a particular x, Na atoms form an ordered arrangement. Zandbergen *et al.*[5] studied various superlattice structures of different γ-Na_xCoO_2 samples by means of transmission electron microscopy (TEM). They proposed ordered Na superlattice models in a wide range of composition ($0.11 < x < 0.75$). Zhang *et al.*[6] and Meng *et al.*[7] calculated the most probable positions of Na which possess the lowest potential energy and predicted ordering patterns of Na for characteristic x values with $0 \leq x \leq 1$ and with $0.5 \leq x \leq 1$, respectively. Such an ordering of Na atoms would influence the electronic states of the CoO_2 layers via its periodic Coulomb potential as described by Roger *et al.*[8] In fact, the phase transition to a charge-ordered (CO) state in the (3+1)-dimensional phase γ-$Na_{0.5}CoO_2$ was explained by the Co-O bond length variation triggered by the cooperative shift of Na at low temperatures.[9]

During the course of research to find another possible phase which exhibits a unique Na ordering, we discovered disorder-order transitions of Na around a composition of γ-Na_xCoO_2 ($x \sim 0.58$). Among the samples, the sample with $x = 0.58$ was found to show the most distinct transition. Here we report the preparation, structural details, and physical properties of γ-$Na_{0.58}CoO_2$.

II. EXPERIMENT

The parent γ-$Na_{0.7}CoO_2$ phase was first synthesized by the standard solid-state reaction method using Na_2CO_3 and Co_3O_4 powders. The γ phase is equivalent to the $P2$-type Na_xCoO_2 compound originally reported by Delmas *et al.*[10] The mixed powders were pelletized and heated twice at 800 °C for 12 h in flowing oxygen with an intermediate grinding. The obtained single-phase powders were then immersed in a CH_3CN-I_2 solution for 48 h with stirring to extract Na^+ ions from the structure. The I_2 concentration was controlled from 0.050 to 0.055 mol/l. After the oxidation, the powders were washed with dehydrated CH_3CN at room temperature several times and then placed in an autodry desiccator for further treatment. An x-ray powder-diffraction measurement was performed to check the formation and purity of the γ-Na_xCoO_2 phase.

The chemical composition of the samples was analyzed with an electron probe microanalysis (EPMA) technique using a JEOL JXA-8621MX instrument. Electron-diffraction (ED) studies were carried out with a JEM-2000EX II TEM operated at 200 kV. Neutron-powder-diffraction (ND) data were collected at several temperatures below 300 K by the use of the Kinken powder diffractometer for high-efficiency and high-resolution measurements (HERMES) (Ref. 11) of the Institute for Materials Research (IMR), Tohoku University, installed at the JRR-3 reactor in Japan Atomic Energy Agency (JAEA), Tokai. A monochromatized incident neutron beam at $\lambda = 1.8265$ Å was employed. The ND data were analyzed using the Rietveld refinement program RIETAN2000.[12] The crystal structure was drawn with VESTA software.[13]

 ©2008 The American Physical Society

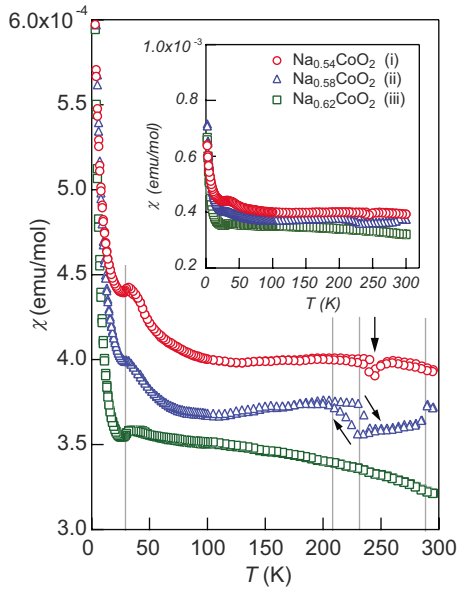

FIG. 1. (Color online) Temperature dependence of the magnetic susceptibility, $\chi(T)$, for Na_xCoO_2 with $x=0.54$, 0.58, and 0.62 samples. The inset shows a $\chi(T)$ plot with a 10^{-3} emu/mol scale.

The magnetic susceptibility of the samples was determined using a quantum design MPMS5 magnetometer under a magnetic field of $H=10\,000$ Oe. Electrical resistivity was measured for the pelletized samples by the standard four-probe method from 5 up to 300 K. The specific heat, C_p, was evaluated using differential scanning calorimetry (DSC) with an SII EXSTAR6000 system from 173 up to 323 K.

III. RESULTS AND DISCUSSION

A. Magnetic susceptibility of Na_xCoO_2 ($x\sim0.58$) samples

Figure 1 shows the temperature dependence of magnetic susceptibility, $\chi(T)$, of three Na_xCoO_2 samples with (i) $x=0.54$, (ii) $x=0.58$, and (iii) $x=0.62$, respectively, determined by means of the EPMA technique. These samples were prepared when the I_2 concentration was 0.055, 0.052, and 0.050 mol/l, respectively; higher I_2 concentration yields lower x samples.

Overall $\chi(T)$ alteration up to 300 K is represented in the inset figure, in which Pauli paramagnetic (PM) behavior is dominantly observed above 50 K. Assuming full oxygen occupancy, the nominal valence state of Co ions is estimated to be 3.46, 3.42, and 3.38 for samples (i), (ii), and (iii), respectively, which indicates that the fraction of magnetic Co^{4+} ($S=1/2$) ions increases with decreasing x. The absolute value of $\chi(T)$ at 300 K slightly increases with decreasing x, attributable to the increase in Co^{4+} concentration. With decreasing temperature T, all the samples exhibit a broad peak at around 30 K and a rapid increase in $\chi(T)$ below 30 K. These broad peaks are quite similar to the ones due to the short-range Ising-type quasi-two-dimensional antiferromagnetic (AF) correlation in $x\sim0.8$ samples.[14] At higher temperature range from 220 to 290 K, the $Na_{0.58}CoO_2$ sample exhibits an anomalous decrease in $\chi(T)$, which involves hysteresis between heating and cooling. A similar anomaly is also observed for the $Na_{0.54}CoO_2$ sample in a narrow temperature range around 240 K (marked with an arrow). In contrast, the $Na_{0.62}CoO_2$ sample shows no anomaly in the same temperature range but shows a weak T-dependent behavior, suggesting that a small amount of Co^{4+} ions are contributing to the Curie-Weiss (CW) term. Recent studies have revealed that the boundary between the "PM metal" and "CW metal" is located at $x\sim0.6$,[15,16] slightly higher than that originally reported by Foo *et al.*[3] at $x=0.5$. Our data also support that the PM-CW boundary is located at $x\sim0.6$. The observed $\chi(T)$ of the three samples implies that the anomalies exist in a relatively narrow Na concentration range at $x\sim0.58$. To study the origin of the magnetic anomaly, we hereafter focus on the physical properties and crystal structure of the $x=0.58$ sample.

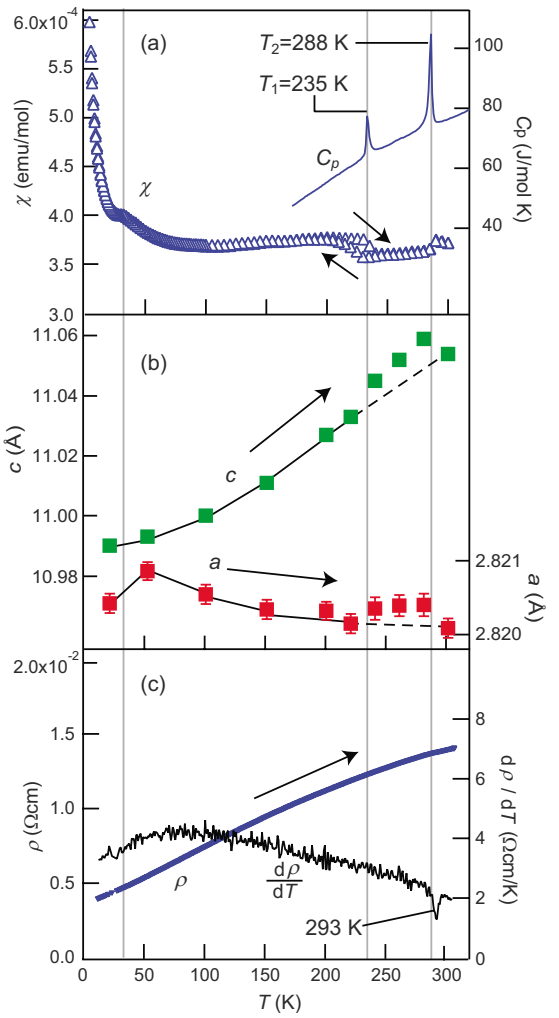

FIG. 2. (Color online) Temperature dependence of (a) magnetic susceptibility, $\chi(T)$ (left), and specific heat, $C_p(T)$ (right), (b) lattice parameters, and (c) electrical resistivity, $\rho(T)$ (left) and its temperature derivative $d\rho(T)/dT$ (right) of $Na_{0.58}CoO_2$.

B. Physical properties and crystal structure of $Na_{0.58}CoO_2$

Figure 2(a) shows the $\chi(T)$ of $Na_{0.58}CoO_2$ measured in the heating and cooling processes, respectively, and $C_p(T)$ in the

TABLE I. Refined lattice parameters, fractional coordinates, occupancies (g) of Na at Na1 and Na2 sites, isotropic displacement parameters (B), and Co-O distances of $Na_{0.58}CoO_2$ based on the "$P6_3/mmc$" model at different temperatures. The atomic positions are Na1: $2b$ (0, 0, 1/4), Na2: $6h$ (x,$2x$,1/4), Co: $2a$ (0, 0, 0), and O: $4f$ (1/3,2/3,z) sites, respectively. The R_{WP} and goodness-of-fit S ($=R_{WP}/R_E$) factors are also listed.

T (K)	22	53	101	151	201	220	240	260	280	300
a (Å)	2.8204(1)	2.8209(1)	2.8206(1)	2.8204(1)	2.8203(1)	2.8202(1)	2.8204(1)	2.8204(1)	2.8204(1)	2.8201(1)
c (Å)	10.9896(4)	10.9931(4)	10.9999(4)	11.0116(4)	11.0267(4)	11.0329(4)	11.0455(4)	11.0525(4)	11.0587(4)	11.0542(4)
g_{Na1}	0.176(7)	0.181(7)	0.174(7)	0.175(7)	0.167(7)	0.176(7)	0.156(8)	0.152(7)	0.161(8)	0.188(8)
g_{Na2}	0.126(3)	0.125(2)	0.123(2)	0.120(2)	0.121(2)	0.119(2)	0.122(3)	0.125(3)	0.121(3)	0.119(2)
x_{Na2}	0.720(3)	0.720(3)	0.722(3)	0.722(3)	0.726(2)	0.723(3)	0.730(3)	0.730(3)	0.731(3)	0.723(3)
B_{Na} (Å^2)	0.4(3)	0.6(3)	0.2(3)	0.6(3)	0.3(3)	0.6(3)	0.5(4)	0.7(4)	0.6(4)	1.1(3)
B_{Co} (Å^2)	0.28(7)	0.14(7)	0.15(7)	0.22(7)	0.32(7)	0.27(7)	0.28(7)	0.35(7)	0.31(8)	0.45(7)
z_O	0.0887(1)	0.0887(1)	0.0888(1)	0.0886(1)	0.0886(1)	0.0885(1)	0.0885(1)	0.0884(1)	0.0885(1)	0.0884(1)
B_O (Å^2)	0.36(3)	0.35(2)	0.36(3)	0.39(3)	0.41(3)	0.42(3)	0.43(3)	0.46(3)	0.49(3)	0.48(4)
$d_{Co\text{-}O}$ (Å)	1.8982(6)	1.8984(6)	1.8989(6)	1.8982(6)	1.8990(6)	1.8989(6)	1.8994(7)	1.8990(7)	1.8999(7)	1.8988(6)
R_{WP} (%)	5.85	5.55	5.62	5.68	5.42	5.51	6.23	6.00	6.19	5.46
S	1.51	1.43	1.45	1.47	1.40	1.43	1.62	1.56	1.61	1.40

heating process. The two peaks in $C_p(T)$ correspond to the temperatures at which the anomalous changes in $\chi(T)$ were observed. These temperatures are assigned as $T_1=235$ K and $T_2=288$ K. The determined enthalpy changes were $\Delta H_{236\ K}=75.0$ J/mol and $\Delta H_{288\ K}=104.8$ J/mol, respectively. The magnitude of $\Delta H_{288\ K}$ is approximately one order smaller than that of a similar layer compound $Ag_{0.36}TiS_2$ ($\Delta H=1540$ J/mol),[17] which undergoes a disorder-order transition of Ag at 286 K. This difference in magnitude of the ΔH implies that both the amount and distance of participating Na atoms in the present phase at the transition would be relatively smaller and shorter than those in $Ag_{0.36}TiS_2$.

In Fig. 2(b), the refined lattice parameters of $Na_{0.58}CoO_2$ are plotted as a function of T. Powder-neutron-diffraction patterns were obtained for the heating process from 22 K. We first assumed the $P6_3/mmc$ space group at all T.[4] Some unindexed peaks, observed at T_1–T_2, which are discussed later, were not excluded in the refinement. With increasing T, the c-axis length increases from 10.9896(4) Å (22 K) to 11.0329(4) Å (220 K) while the a-axis length slightly increases from 2.8204(1) Å (22 K) to 2.8209(1) Å (53 K). With further increasing T, the a-axis length begins to decrease gradually and reaches 2.8202(1) Å at 220 K. Between T_1 and T_2, both the a- and c-axes lengths are longer relative to the values extrapolated from the ones below T_1 and 300-K data (dashed line). The refined lattice parameters, as well as the fractional coordinates, occupancies of Na1 and Na2 sites, isotropic displacement parameters B, and Co-O distances, obtained by assuming the "$P6_3/mmc$" space group, are summarized in Table I. During the refinement, the B parameters of identical atoms were constrained to be equal. Note that the R_{WP} and goodness-of-fit S are rather high at 240–280 K, due to unindexed small peaks. Despite the irregular elongation in the a-axis length, the determined Co-O bond distances show no significant change over the entire range of T, based on this model. Further discussion on the Co-O distances will be given in Sec. III C.

Figure 2(c) shows the temperature dependence of electrical resistivity, $\rho(T)$, and its temperature derivative $d\rho(T)/dT$ of $Na_{0.58}CoO_2$, measured in the heating process. At $T=5$ K, the sample shows $\rho=3.8$ mΩ cm and exhibits metallic behavior up to 300 K. Such a metallic resistivity below the magnetic transition temperature is not observed for the samples with higher Na content described above,[14] while similar $\chi(T)$ behavior is observed. Thus, the origin of the broad $\chi(T)$ peak at $T\sim30$ K followed by the steep increase at lower T in our sample should be essentially different from the $x\sim0.8$ samples; the $\chi(T)$ behavior below 30 K in our sample is, most possibly, due to a paramagnetic impurity which was not detected in the ND patterns. With increasing T, the $\rho(T)$ curve shows some concave behavior at $T=80$–100 K, where a broad minimum in the $\chi(T)$ curve is recognized. Similar behavior is frequently observed for the layered cobaltates in which the carrier scattering mechanism is dominated by the quasielastic regime at low T to a phonon scattering one at highest T.[18] According to the temperature dependence of $d\rho(T)/dT$, no discernible anomaly was observed at T_1, but was observed at T_2.

C. Structure details of $Na_{0.58}CoO_2$

Figures 3(a) and 3(b) show the ED patterns of $Na_{0.58}CoO_2$

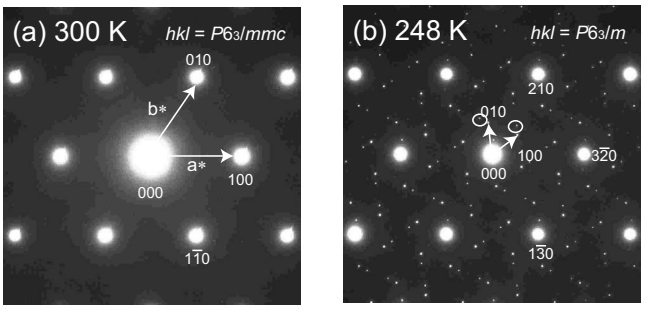

FIG. 3. Electron diffraction patterns of $Na_{0.58}CoO_2$ taken with incident electron beam parallel to [001], measured at (a) 300 and (b) 248 K.

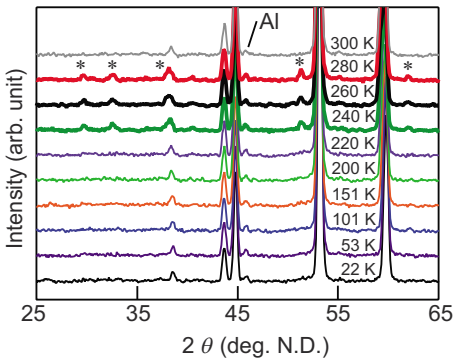

FIG. 4. (Color online) Observed powder-neutron-diffraction patterns for $Na_{0.58}CoO_2$ measured at 22, 53, 101, 151, 200, 220, 240, 260, 280, and 300 K. The peaks marked with "*" and "Al", respectively, correspond to the superlattice peaks observed in Fig. 3(b) and the peak of the aluminum sample can.

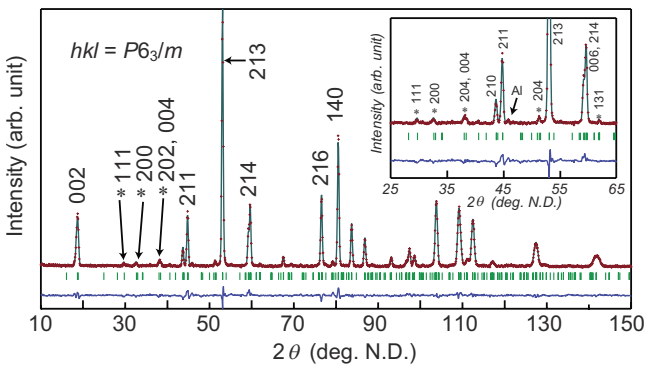

FIG. 5. (Color online) Observed, calculated, and difference patterns of powder-neutron-diffraction data for $Na_{0.58}CoO_2$ measured at 280 K. The peaks marked with "*" and "Al", respectively, correspond to the unindexed peaks assuming $P6_3/mmc$ space group and the peak of aluminum sample can.

measured at 300 and 248 K, respectively, taken with the incident beam parallel to the c axis. At 300 K, the diffraction pattern consists of only strong spots with sixfold symmetry, typically observed for the γ-Na_xCoO_2 ($P6_3/mmc$) phase with randomly occupied Na sites. At 248 K, many additional small spots appear in the ED pattern, being similar to the case of incommensurate $Ag_{0.6}NbS_2$.[19] Such an incommensurate ED pattern was analyzed assuming a (3+2)-dimensional superspace-group symmetry by Lee *et al.*[19] The glimmers in our ED pattern (marked with circles) also imply the first-order satellite reflection and modulated structure. However, every spot at 248 K is approximately indexed assuming a simple commensurate three-dimensional $\sqrt{7}a_0 \times \sqrt{7}a_0$ superlattice structure [Fig. 3(b)]. To investigate the detailed structure, we first assumed the $\sqrt{7}a_0 \times \sqrt{7}a_0$-type Na-ordering model originally proposed by Zhang *et al.*[6] for $Na_{0.60}CoO_2$ composition. In this case, we were unable to obtain a reasonable solution for our $Na_{0.58}CoO_2$ sample. Instead, a successful analysis was achieved on the basis of an ordered-structure model, isostructural with $K_4Co_7O_{14}$ ($P6_3/m$), reported by Blangero *et al.*[18]

Figure 4 illustrates the temperature evolution of ND patterns for the $Na_{0.58}CoO_2$ sample measured at 22–300 K. Similar to the ED patterns, the ND patterns also possess additional small peaks at 240, 260, and 280 K (marked with "*" in the figure), which correspond to the small spots in Fig. 3(b). In contrast, there is no unindexed peak at $T < T_1$ and $T > T_2$, suggesting that the structure of $Na_{0.58}CoO_2$ at $T < T_1$ is identical or close to the one at $T > T_2$. Between T_1 and T_2, we regarded that the structure of the sample is maintained to be the $\sqrt{7}a_0 \times \sqrt{7}a_0$ type. Figure 5 represents the observed difference profiles of the HERMES data for $Na_{0.58}CoO_2$ measured at 280 K and the fitted curve calculated with the $\sqrt{7}a_0 \times \sqrt{7}a_0$ ($P6_3/m$) model. The short vertical lines show the peak positions of possible Bragg reflections. The inset figure shows the enlarged pattern at $2\theta = 25° - 65°$. All the small unindexed peaks with $P6_3/mmc$ (the peaks marked with "*" in Fig. 4) are now indexed assuming the Blangero's $P6_3/m$ model.[18] Hence, it is concluded that $Na_{0.58}CoO_2$ has a $K_4Co_7O_{14}$-type structure ($K_{0.57}CoO_2$) at 280 K. The final R_{WP} and S reach 5.83% and 1.52, respectively, being reasonably lower than those of the $P6_3/mmc$ model presented in Table I. Similarly, ND patterns measured at 260 and 240 K were successfully analyzed using the same model. Table II summarizes the refined structural parameters of the Rietveld analysis at 240, 260, and 280 K.

Figures 6(a) and 6(b) show the c-axis projections near $z = 1/4$ of the refined $Na_{0.58}CoO_2$ structure at (a) 300 and (b)

TABLE II. Refined structural parameters of $Na_{0.58}CoO_2$ between T_1 and T_2 based on the $P6_3/m$ model (Ref. 18). The atomic positions are Na1: 2a (0, 0, 1/4), Na2: 6h (x,y,1/4), Co1: 2b (0, 0, 0), Co2: 12i (x,y,z), O1: 12i (x,y,z), O2: 12i (x,y,z), and O3: 4f (1/3,2/3,z) sites, respectively. The occupation factor of each atom is fixed at 1.0. The R_{WP} and goodness-of-fit S ($=R_{WP}/R_E$) factors are also listed.

T (K)	240	260	280
a (Å)	7.4621(4)	7.4622(3)	7.4622(4)
c (Å)	11.0453(4)	11.0524(4)	11.0585(4)
x_{Na2}	0.449(3)	0.451(2)	0.449(2)
y_{Na2}	0.390(2)	0.389(2)	0.391(2)
B_{Na} (Å^2) [a]	2.8(2)	3.2(2)	3.1(2)
x_{Co2}	0.282(2)	0.280(2)	0.282(2)
y_{Co2}	0.426(2)	0.426(2)	0.426(2)
z_{Co2}	−0.008(1)	−0.008(1)	−0.009(1)
B_{Co} (Å^2) [a]	0.22(8)	0.26(8)	0.22(8)
x_{O1}	0.238(1)	0.238(1)	0.239(1)
y_{O1}	0.190(2)	0.192(2)	0.192(2)
z_{O1}	0.0895(6)	0.0894(6)	0.0893(6)
x_{O2}	0.0960(10)	0.0956(9)	0.0960(10)
y_{O2}	0.480(1)	0.479(1)	0.479(1)
z_{O2}	0.0852(4)	0.0854(4)	0.0853(4)
z_{O3}	−0.094(1)	−0.093(1)	−0.094(1)
B_O (Å^2) [a]	0.30(3)	0.33(3)	0.36(3)
R_{WP} (%)	5.74	5.56	5.83
S	1.50	1.45	1.52

[a] B factors of identical atoms were constrained to be equal with each other.

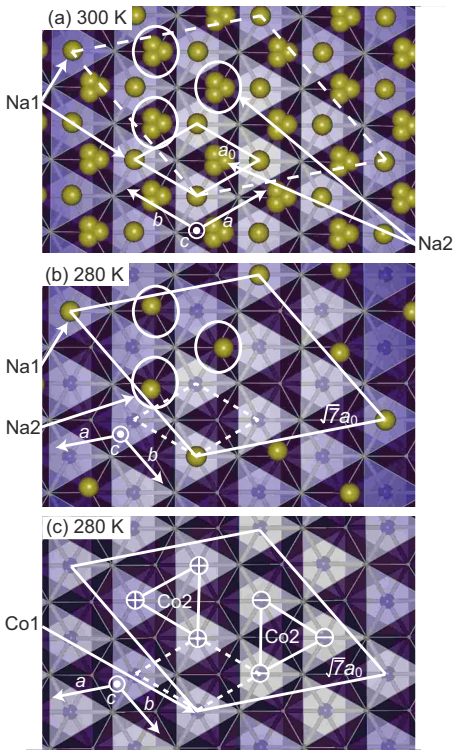

FIG. 6. (Color online) Revealed crystal structure of $Na_{0.58}CoO_2$ at (a) 300 and (b) 280 K, viewed parallel to the z direction with the region of $-0.1 \leq z \leq 0.25$. O atoms are omitted from the figures for simplicity. The cooperative shift of Co2 atoms at $z \sim 0$ is drawn in (c). The "+" and "−" marks in the circles, respectively, indicate z coordinate of Co2 atoms at $z=+0.10(1)$ and $z=-0.10(1)$.

280 K. The solid rhombuses in Figs. 6(a) and 6(b) represent the unit cells at 300 and 280 K, respectively. The dashed rhombuses in those figures show those at 280 and 300 K. At 300 K, the Na2 site has three equivalent positions with the occupation factor of $g_{Na2}=0.119(2)$ as shown in Table I; each equivalent position in a circle is statistically occupied with the probability of ~12%. Similarly, the Na1 site is statistically occupied with the probability of ~19%. The determined total Na content in the formula, i.e., $x=\frac{1}{2}(2\times g_{Na1}+6\times g_{Na2})=0.55(1)$, well agrees with the analyzed one of 0.58. At 280 K, in contrast, the $\sqrt{7}a_0\times\sqrt{7}a_0$-type unit cell allows the full occupancy for both Na1 and Na2 sites. The Na1 atom is located at the 2*a* (0, 0, 1/4) site and the Na2 site being at positions shown as circles in Fig. 6(b). Hence, the randomly distributed Na atoms at higher T must move to these positions below T_2 to form the ordered arrangement of Na atoms.

Based on the refined structure, the ideal chemical composition of the ordered phase is formulated as $Na_4Co_7O_{14}$ ($Na_{0.57}CoO_2$). As the present $x=0.58$ sample has the close stoichiometry to this composition, the sample may easily transform to the $\sqrt{7}a_0\times\sqrt{7}a_0$-type structure at a certain temperature range, where the Na-ordered phase is energetically favorable than that of the disordered high-temperature phase. As described, the $Na_{0.54}CoO_2$ sample also shows a similar transition but the transition was limited at a narrow temperature range around 240 K. We consider that the Na content of

TABLE III. Determined Co-O bond distances (Å) of $Na_{0.58}CoO_2$ between T_1 and T_2 based on the $P6_3/m$ model (Ref. 18).

T (K)	240	260	280
Co1-O1 ×6	1.905(7)	1.907(7)	1.911(7)
$Co2^a$-$O1^a$ ×1	1.941(17)	1.936(18)	1.938(18)
$Co2^a$-$O1^d$ ×1	1.837(17)	1.841(17)	1.836(17)
$Co2^a$-$O2^a$ ×1	1.928(17)	1.917(16)	1.935(17)
$Co2^a$-$O2^b$ ×1	1.925(15)	1.941(15)	1.937(15)
$Co2^a$-$O2^c$ ×1	1.860(15)	1.869(16)	1.852(16)
$Co2^a$-$O3^a$ ×1	1.897(17)	1.885(18)	1.892(18)

[a] x,y,z symmetry operator.
[b] $\bar{x}+1/2,y,z$ symmetry operator.
[c] $y,\bar{x}+y,\bar{z}$ symmetry operator.
[d] $x-y,x,\bar{z}$ symmetry operator.

$x=0.54$ is not high enough to totally transform into the $\sqrt{7}a_0\times\sqrt{7}a_0$-type structure; the distribution of Na atoms may be inhomogeneous at ~240 K and only the Na-rich regions show such a Na ordering.

In the $\sqrt{7}a_0\times\sqrt{7}a_0$-type structure of $Na_{0.58}CoO_2$, there are two crystallographic sites for Na and Co atoms and three sites for O atoms. The Co1 atom is only bonded to six equivalent O1 atoms and the Co1-O bonds have an identical distance 1.911(7) Å at 280 K. However, the positions of the Co2 atoms slightly shift upward and downward from $z=0$ (~±0.10 Å) due to the Na ordering as shown in Table II. Consequently, each Co2-O bond becomes inequidistant as shown in Table III. At 280 K, the Co2-O bond lengths are in the range from 1.836(17) to 1.938(18) Å, forming a distorted CoO_6 octahedron. The observed enthalpy change in the present phase, $\Delta H_{288\ K}$, accounts for the energy required for this redistribution of the Na atoms and a slight shift of the Co atoms. The shifted Co2 atoms form a trimer with the same z coordination (+) or (−) while Co1 atoms remain unshifted, causing undulated Co lattices [two triangles in Fig. 6(c)]. The slight decrease in $\chi(T)$ observed in Fig. 1 can be attributed to the cooperative shift of the Co2 trimers.

Finally, it would be of interest to compare the crystal structure and transport properties between $Na_{0.58}CoO_2$ and its K analog, $K_4Co_7O_{14}$. Both the compounds exhibit metallic $\rho(T)$ and Pauli paramagnetic $\chi(T)$ behavior below room temperature.[18,20] Moreover, the magnitudes of $\rho(T)$ and $\chi(T)$ are comparable for these compounds. However, the $Na_{0.58}CoO_2$ phase evolves the disorder-order transition at T_1 and T_2 and the long-range magnetic order at around 30 K. Reflecting the difference in ionic radii of Na and K, the reported lattice parameters of $K_4Co_7O_{14}$ at room temperature, $a=7.5171(1)$ Å and $c=12.371(1)$ Å, are much longer than those of the Na-ordered $Na_{0.58}CoO_2$ phase of $a=7.4622(4)$ Å and $c=11.0585(4)$ Å at 280 K. Thus, the two-dimensionality can be much stronger in the $K_4Co_7O_{14}$ phase. In addition, the positional shift of Co2 sites along the z direction is only ±0.032 Å in the K phase, which is approximately 1/3 of that in the Na-ordered $Na_{0.58}CoO_2$ phase. Such a small undulation of Co2 sites would cause negligibly little effect on the transport properties even if there is a pos-

sible structural change into a K-disordered phase.

IV. SUMMARY AND CONCLUSION

A type of Na ordering in the Na_xCoO_2 series was discovered at $x=0.58$ in the temperature range of $T_1=235$ K to $T_2=288$ K. In the $\sqrt{7}a_0\times\sqrt{7}a_0$ ordered phase, the space group is changed from $P6_3/mmc$ to $P6_3/m$ and the CoO_2 layer is slightly distorted, triggered by the Na ordering. The electrical resistivity, magnetic susceptibility, and specific heat exhibit anomalous behavior at T_1 and T_2. However, a reasonable interpretation for the elimination of superlattice peaks at $T<T_1$ has not yet been achieved. For further understanding, detailed structure analysis of the phase at $T<T_1$ is currently underway.

ACKNOWLEDGMENTS

We thank K. Nemoto for technical assistance in the HERMES experiment and Y. Kasai at SII for specific-heat measurement by DSC. This study was partly supported by the Core Research for Evolution Science and Technology (CREST) Project of the Japan Science and Technology Agency (JST), and also by a Grant-in-Aid for Scientific Research from the Ministry of Education, Culture, Sports, Science and Technology, Japan.

*dai@crystal.apph.tohoku.ac.jp

[1] I. Terasaki, Y. Sasago, and K. Uchinokura, Phys. Rev. B **56**, R12685 (1997).
[2] K. Takada, H. Sakurai, E. Takayama-Muromachi, F. Izumi, R. A. Dilanian, and T. Sasaki, Nature (London) **422**, 53 (2003).
[3] M. L. Foo, Y. Wang, S. Watauchi, H. W. Zandbergen, T. He, R. J. Cava, and N. P. Ong, Phys. Rev. Lett. **92**, 247001 (2004).
[4] Y. Ono, R. Ishikawa, Y. Miyazaki, and T. Kajitani, J. Phys. Soc. Jpn. **70**, Suppl. A, 235 (2001).
[5] H. W. Zandbergen, M. Foo, Q. Xu, V. Kumar, and R. J. Cava, Phys. Rev. B **70**, 024101 (2004).
[6] P. Zhang, R. B. Capaz, M. L. Cohen, and S. G. Louie, Phys. Rev. B **71**, 153102 (2005).
[7] Y. S. Meng, Y. Hinuma, and G. Ceder, J. Chem. Phys. **128**, 104708 (2008).
[8] M. Roger, D. J. P. Morris, D. A. Tennant, M. J. Gutmann, J. P. Goff, J.-U. Hoffmann, R. Feyerherm, E. Dudzik, D. Prabhakaran, A. T. Boothroyd, N. Shannon, B. Lake, and P. P. Deen, Nature (London) **445**, 631 (2007).
[9] D. Igarashi, Y. Miyazaki, K. Yubuta, and T. Kajitani, Jpn. J. Appl. Phys., Part 1 **46**, 304 (2007).
[10] C. Delmas, C. Fouassier, and P. Hagenmuller, Physica B & C **99**, 81 (1980).
[11] K. Ohoyama, T. Kanouchi, K. Nemoto, M. Ohashi, T. Kajitani, and Y. Yamaguchi, Jpn. J. Appl. Phys., Part 1 **37**, 3319 (1998).
[12] F. Izumi and T. Ikeda, Mater. Sci. Forum **198**, 321 (2000).
[13] K. Momma and F. Izumi, J. Appl. Crystallogr. **41**, 653 (2008).
[14] S. P. Bayrakci, C. Bernhard, D. P. Chen, B. Keimer, R. K. Kremer, P. Lemmens, C. T. Lin, C. Niedermayer, and J. Strempfer, Phys. Rev. B **69**, 100410(R) (2004).
[15] M. Yokoi, T. Moyoshi, Y. Kobayashi, M. Soda, Y. Yasui, M. Sato, and K. Kakurai, J. Phys. Soc. Jpn. **74**, 3046 (2005).
[16] D. Yoshizumi, Y. Muraoka, Y. Okamoto, Y. Kikuchi, J. Yamaura, M. Mochizuki, M. Ogata, and Z. Hiroi, J. Phys. Soc. Jpn. **76**, 063705 (2007).
[17] H. Fujimori, M. Oguni, K. Kitayama, T. Uchida, and M. Wakihara, J. Phys.: Condens. Matter **5**, 6673 (1993).
[18] M. Blangero, R. Decourt, D. Carlier, G. Ceder, M. Pollet, J. P. Doumerc, J. Darriet, and C. Delmas, Inorg. Chem. **44**, 9299 (2005).
[19] A. van der Lee, S. van Smaalen, G. A. Wiegers, and J. L. de Boer, Phys. Rev. B **43**, 9420 (1991).
[20] J. Sugiyama, Y. Ikedo, P. L. Russo, H. Nozaki, K. Mukai, D. Andreica, A. Amato, M. Blangero, and C. Delmas, Phys. Rev. B **76**, 104412 (2007).